LAWRENCE
LIVERMORE
NATIONAL
LABORATORY

LLNL-JRNL-859208

Experimental and modeling study of the effect of confinement on the thermal decomposition of organic materials

C. Saggese, A. K. Burnham

January 16, 2024

Thermochimica Acta

Disclaimer

This document was prepared as an account of work sponsored by an agency of the United States government. Neither the United States government nor Lawrence Livermore National Security, LLC, nor any of their employees makes any warranty, expressed or implied, or assumes any legal liability or responsibility for the accuracy, completeness, or usefulness of any information, apparatus, product, or process disclosed, or represents that its use would not infringe privately owned rights. Reference herein to any specific commercial product, process, or service by trade name, trademark, manufacturer, or otherwise does not necessarily constitute or imply its endorsement, recommendation, or favoring by the United States government or Lawrence Livermore National Security, LLC. The views and opinions of authors expressed herein do not necessarily state or reflect those of the United States government or Lawrence Livermore National Security, LLC, and shall not be used for advertising or product endorsement purposes.

Experimental and modeling study of the effect of confinement on the thermal decomposition of organic materials

Chiara Saggese[a,*], Alan Burnham[a,b]
[a]*Lawrence Livermore National Laboratory, Livermore, CA 94550, United States*
[b]*Stratify//MH Chew Associates, 7633 Southfront Road, Ste. 170, Livermore, CA 94551, United States*

*Corresponding author
Chiara Saggese
Materials Science Division
Lawrence Livermore National Laboratory
Email: saggese1@llnl.gov
Phone: +1-925-423-4254

Type of article: Full length
For printed editions, the authors request that color figures are converted to black and white.

Submitted for publication in Thermochimica Acta

February 9, 2024

Abstract

Simultaneous Thermal Analysis is widely used to study thermal decomposition of a variety of organic materials, and the choice of experimental conditions is very important to obtain reliable mass loss and heat flow curves. In this work we investigate the effect of confinement on the thermal decomposition of organic materials. As an example, we explore high-density polyethylene (HDPE) and one of its pyrolysis products, namely eicosane ($C_{20}H_{42}$), through experiments and modeling in open crucibles and crucibles closed with a pierced lid. A new model is developed for evaporation and sublimation from open and pinhole thermal-analysis pans. It considers the kinetic resistance of evaporation at the liquid-vapor interface, inhibition of evaporation by buildup of vapor inside the pan, thermal expansion of vapor inside the pan, and diffusion of vapor from the pan. The model is validated using simultaneous heat-flow and mass-loss measurements of n-eicosane evaporation for various pinhole sizes, down to 50 µm. The importance of product evaporation inhibition for measuring polymer decomposition was demonstrated using HDPE. This study sheds light on the effect of confinement on the mass loss rate of organic materials.

Keywords: diffusion, evaporation, thermogravimetric analysis, eicosane, pan with pierced lid

1. Introduction

The thermal decomposition of organic compounds is a multi-phase phenomenon. Some of these substances decompose in liquid form while simultaneously vaporizing. Others decompose in the solid phase and may be accompanied by sublimation, which has a profound effect on the overall kinetics. Also, evaporation of primary products may be inhibited by low vapor pressure, thereby increasing secondary reactions.

Simultaneous Thermal Analysis (STA) is commonly used to study thermal decomposition of a variety of solid/organic materials, including wood, polymers, and energetic materials [1]. STA combines Thermogravimetric Analysis (TGA) and Differential Scanning Calorimetry (DSC) to measure and examine the sample weight loss and the temperature dependent heat-release rates. The choice of proper experimental conditions is crucial because the difference in sample mass, crucible type, heating rate, and surrounding atmosphere can significantly impact the mass-loss or heat-flow curves. Specifically, careful choice of the crucible type is important for collecting significant experimental data. The usual selection of crucible type ranges between a hermetically closed crucible, a crucible with pierced lid, and an open crucible, which represent different levels of sample confinement.

In the literature, many groups have investigated some of these STA operating parameters, such as the heating rate or the surrounding atmosphere, and their effect on the thermal decomposition of organic compounds is well known [2-4]. However, studies on the effect of confinement on thermal decomposition of organic materials are rather limited.

Wolfinger et al. [5] and Rath et al. [6] were among the first to investigate the effect of the presence of a lid on the crucible on calorimetric measurements of the heat of pyrolysis of biomass. They observed differences in mass loss and heat flow profiles with and without lid. They claimed that the presence of a lid caused the decomposition process to change from endothermic to exothermic, because secondary char formation reactions became dominant at low temperatures. Recently, Anca-Couce et al. [7] developed a model to explain the measurements of heat flow in micro-TGA-DSC experiments of biomass pyrolysis. They studied the biomass thermal decomposition in an open crucible and also using a lid to confine the sample. They found that secondary reactions are enhanced in the presence of the lid and the global heat of reaction shifts from endothermic to exothermic. Similar findings were recently reported by Torres-Herrador et al. [8], who showed that covering the crucible with a pierced lid during the pyrolysis of a carbon/phenolic thermal protection material enhances char formation compared to the open crucible case, and by Lazaro et al. [9], who showed that the use of the lid increased the final char yield of poly (vinyl chloride) (PVC) decomposition.

Thermal decomposition experiments of energetic materials are usually carried out with closed crucibles or crucibles with pierced lid to control better the process and have reliable measurements. A few studies have investigated the effect of pinholes on thermal decomposition

and sublimation behaviors of energetic materials. Long et al. [10] explored competitive evaporation and decomposition of 1,3,5-trinitro-1,3,5-triazinane (RDX) in open and pinhole pans. Weese et al. [11] showed that 2,6-diamino-3,5-dinitropyrazine-1-oxide (LLM-105) sublimed in an open pan and decomposed in a pinhole pan. Most recently, Koroglu et al. [12] explored the effect of the pinhole size on 1,3,5-triamino-2,4,6-trinitro benzene (TATB) thermal decomposition and sublimation through STA measurements. They found that decreasing the pinhole size for a given starting mass and heating rate caused an increase in the enthalpy of reaction. Correspondingly, when the maximum heat flow and weight loss are reached, the amount of residue and the peak temperatures increase as well. In addition, Gorn et al. [13] showed an increased suppression of evaporation relative to the decomposition of 3,4-dinitropyrazole by increasing pressure.

The objective of this work is to understand how to properly analyze thermal analysis data for the decomposition of materials when the extent of reaction, including potential competition between evaporation and decomposition reactions, and the degree of secondary gas-phase reactions depend on the type of crucible used. For these reasons, herein we study the effect of confinement on the decomposition of high-density polyethylene (HDPE) and one of its pyrolysis products, namely eicosane ($C_{20}H_{42}$), through experiments and modeling. A new fast-running model has been developed to account for vapor and liquid mass loss with various degrees of confinement, including various pinhole sizes.

The goal is to better understand the interplay between the various processes happening during STA experiments with open crucible and crucible with pierced lid, such as evaporation, gas diffusion through the pinhole and gas advection outside the crucible.

Additionally, the fast-running model herein developed can be used to interpret experiments in crucible with pierced lid, including for energetic materials, where there is a competition between evaporation and decomposition and where confinement of volatile primary products affects the rate of autocatalytic reactions.

2. Experiments

2.1 Eicosane experiments

Samples of eicosane (99% purity; CAS n. 112-95-8) were purchased by Sigma Aldrich. They were used without any further purification. Evaporation experiments were conducted on a Mettler-Toledo (MT) Thermal Analysis System TGA/DSC 3+ at multiple heating rates of 1, 10, 20, 60 K/min using N_2 as a purge gas at 80 ml/min. Table 1 depicts the operating conditions for the eicosane experiments. The experiments were performed at atmospheric conditions. For most experiments, between 0.25 and 2.14 mg of eicosane were loaded into MT 40-µl Al pans. The

smallest pinhole lids used were purchased from MT and were nominally 50 μm in diameter. Other pinholes were created with needles, and the diameters were verified by microscopy. For the experiments 8-11 and 12-14, 40-μl Al pans from TA Instruments were used. Two additional open pan experiments using 1.08 mg of eicosane and purge-gas flowrates of 40 and 120 ml/min were conducted, and it was observed that evaporation was not affected by the purge-gas flowrate, as shown in Fig. S1 of the Supplemental Materials.

Table 1
Operating conditions (heating rate, pinhole size, and starting mass) and fitted values of diffusion path length z for eicosane experiments.

Test no.	Heating rate [K/min]	Pinhole diameter size [mm]	Starting mass [mg]	Diffusion path length [mm]
1	1	4.6 (open)	1.03	0.8
2		0.35	0.34	0.4
3		0.35	1.07	0.4
4		0.35	1.98	0.45
5		0.05	0.34	0.07
6		0.05	1.09	0.1
7		0.05	1.98	0.1
8	10	4.6 (open)	0.57	0.8
9		4.6 (open)	0.89	0.8
10		4.6 (open)	1.05	0.8
11		4.6 (open)	1.21	0.8
12		0.8	0.59	0.7
13		0.8	0.92	0.9
14		0.8	1.24	0.7
15		0.35	0.49	0.5
16		0.35	1.07	0.5
17		0.35	2.01	0.5
18		0.05	0.25	0.15
19		0.05	0.49	0.12
20		0.05	1.02	0.15
21		0.05	2.14	0.2
22	20	1	1.89	0.7
23		1	2.04	0.85
24		1	2.12	0.9
25	60	4.6 (open)	0.43	0.8
26		4.6 (open)	0.49	0.8

2.2 HDPE experiments

High-Density Polyethylene (HDPE) was obtained from Sigma Aldrich. It had an average molecular weight of 3-6 million Daltons and a melting point of 138 °C. About 1.6 mg of material was shaved from larger pieces and placed in 40-µL MT pans. Some of the pans were covered with pierced lids with pinholes of varying diameter, as shown in Table 2. Replicates were measured for open pans and for 0.35-mm and 0.05-mm pinholes.

Table 2
Operating conditions (heating rate, pinhole size, and starting mass) for HDPE experiments.

Test no.	Heating rate [K/min]	Pinhole diameter size [mm]	Starting mass [mg]
1	10	4.6 (open)	1.60
2		1.4	1.57
3		1.0	1.70
4		0.35	1.55
5		0.05	1.55

3. Modeling

In the thermal analysis experiments we conducted the sample was positioned in an open or pierced cylindrical pan, surrounded by a flow of inert purge-gas (N_2), which removed all the vapors from the sample pan, as shown in Fig.1. The sample mass loss, which is measured thermogravimetrically, is caused by the evaporation of the sample (1), the successive gas expansion (2), and the diffusion of the gas into the surrounding atmosphere (3).

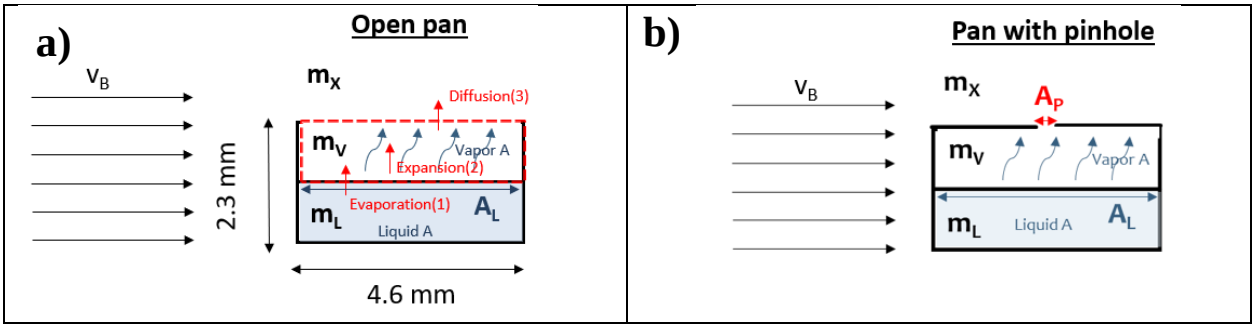

Fig. 1. Schematic of the open pan (panel a) and pinhole-pan (panel b) thermal analysis experiments. The processes occurring are: (1) evaporation, (2) gas expansion, and (3) gas diffusion into the atmosphere.

In literature, there are various approaches to model the mass-loss rate in TGA experiments. Usually, for open-pan experiments, the mass loss due to evaporation follows the Langmuir

relation [14], which was revised by Pieterse and Focke [15] to consider the diffusion of the sample gas into the atmosphere, and it is described by the expression:

$$\frac{dm_A}{dt} = \frac{M_A * S}{R * T} * P_A * D_{AB} \quad (1)$$

Here dm_A/dt g s^{-1} is the rate of mass loss; P_A (Pa) is the sample vapor pressure at absolute temperature T (K); R (J mol^{-1} K^{-1}) is the gas constant; D_{AB} (m^2 s^{-1}) is the binary diffusion coefficient for the vaporizing compound A in the purge gas B; M_A (kg $kmol^{-1}$) is the molar mass of the vaporizing compound; and S (m) is a shape factor dependent on the system geometry.

Frequently, the system geometry in thermogravimetric experiments is represented by a cylindrical pan partially filled with sample having an inert purge gas flowing over the top. In this case, $S = A/z$, where A (m^2) is the cross-sectional surface area and z (m) is the characteristic length over which a significant concentration gradient exists so that diffusion results in a net max flux out of the reaction zone. Later, many authors [16-19] tried to account for the impact of the purge-gas flow on the mass loss rate. For instance, Heym et al. [18] calculated the mass transfer coefficient using a new correlation for the Sherwood number for cylindrical crucibles. However, our experiments were independent of the purge-gas flowrate, hence Sherwood number (see Fig. S1 of the Supplemental Materials).

For the system here considered, substance A corresponds to eicosane ($C_{20}H_{42}$) and the purge gas is N_2.

We model the mass loss of eicosane considering three main variables: m_L (liquid mass), m_V (vapor mass inside the pan) and m_X (vapor mass which exited the pan). For the mass conservation law, we have:

$$m_x + m_V + m_L = constant \quad (2)$$

The evolution of the liquid mass (m_L) is controlled by evaporation (1):

$$\frac{dm_L}{dt} = -k_V * MW_A * A_L * \left(\frac{m_L}{m_L(0)}\right)^{0.2} * \left(1 - \frac{P_v}{P_e}\right) \quad (3)$$

where k_v (mol m^{-2} s^{-1}) is the kinetic constant of evaporation; MW_A (g mol^{-1}) is the molecular weight of eicosane; A_L (m^2) is the liquid area of eicosane, $m_L(0)$ is the initial liquid mass, P_v is the partial pressure of eicosane in the headspace calculated following the ideal gas law; P_e is the equilibrium vapor pressure of eicosane at temperature T derived through the Antoine equation. In the absence of more definitive information, we have chosen the simplest form to make the evaporation rate go to zero when the gas-phase becomes saturated with vapor. [20]

We first derived estimates for k_v in Arrhenius form by fitting the data for 1 mg of eicosane evaporated from open pans at heating rates of 1 and 10 K/min, using both Kissinger's equation (E_a=84.6 kJ/mol; A=3.1×10^6 mol m^{-2} s^{-1}) and an nth-order reaction (E_a=83.4 kJ/mol; A=2.50×10^6 mol m^{-2} s^{-1}; n = 0.2). Evaporation from a flat surface is formally a zero-order, but it is likely that there is some puddling as the amount of material approaches zero and therefore, we have n=0.2.

However, these initial estimates do not explicitly consider diffusion resistance and the higher temperatures of the pinhole experiments. Since the enthalpy of evaporation depends on temperature due to the differences in heat capacity in the liquid and vapor phases [21], an enthalpy (i.e. E_a) more appropriate for the higher temperatures associated with pinhole experiments was determined. From the ratio of the peak heat flow and mass loss rate in experiments 22-24, we obtained an E_a value of 71.2 kJ/mol. This agrees with the NIST database trends [22]. Details are given in Section 2 of the Supplemental Materials. Current Arrhenius values used in the model for k_v are E_a=72 kJ/mol and A=2.50×10^5 mol m^{-2} s^{-1}, which are close to the ones obtained from the fitting of the experimental data and consider also the higher temperatures associated with pinhole experiments. The k_v rates calculated from these final A and E_a values are equal at 322.4 °C to those obtained from the initial kinetic analysis.

To consider the change in the partial pressure of the vapor that exists above the surface (P_v) due to the various levels of confinement, we added the term (1-P_v/P_e) to Eq. 3. As well explained in Lewczyk et al. [23], an equilibrium is reached in a sealed container and P_e = P_v, such that there is no net loss of mass from the surface. In contrast, in a dynamic vacuum, the equilibrium is not reached, and P_v approaches 0, such that a maximum rate of mass loss can occur. The open pan under an inert gas flow in a TGA instrument exists between these two extremes, and it is common to express the process using Eq. 1. However, for our experiments we need to add the term (1-Pv/Pe), which is bounded by 0 and 1 and corresponds to equilibrium and to unidirectional removal from the surface, respectively.

The vapor mass (m_V) time history inside the pan depends on various processes, such as evaporation from the liquid (1), gas expansion due to continued heating of the pan (2) and diffusion of the gas from the headspace to the outside the pan in the surrounding atmosphere (3):

$$\frac{dm_V}{dt} = \left(1 - \frac{P_v}{P_t}\right) * \left(k_V * MW_A * A_L * \left(\frac{m_L}{m_{L(0)}}\right)^{0.2} * \left(1 - \frac{P_v}{P_e}\right)\right) - \frac{m_V}{T} * \frac{dT}{dt} - \frac{MW_A * A_P * P_v * D_{AB}}{z * R * T} \qquad (4)$$

where P_t is the total pressure (1 atm); A_P (m^2) is the pinhole area; D_{AB} (cm^2 s^{-1}) is the binary diffusion coefficient of eicosane in vapor N_2; z (m) is the diffusion path length, that is the characteristic length over which diffusion happens.

The three terms used to represent the vapor mass time history inside the pan are:

- the first term represents the vapor evaporated from the liquid. The term (1-P_v/P_t) represents the effect of the pressure of gaseous products on the reversible decomposition rate [20, 24];

- the second term accounts for vapor expansion due to increasing temperature;
- the third term considers diffusion of the gas from the pan to the outside, which is a function of the diffusion coefficient D_{AB} and the diffusion path length z.

The diffusion coefficient of eicosane in N_2 ($D_{C20H42-N2}$) can be estimated in different ways. The semi-empirical Fuller correlation [25] is usually adopted in thermogravimetric studies, which has a dependency on temperature of $T^{1.75}$. In this work we used the correlation from the work of Chae et al. [26], derived from molecular dynamics simulations used to compute binary diffusion coefficients of linear alkanes up to C16 over the temperature range 500-1000 K, which we extended to C20 thus obtaining a temperature dependency of $T^{1.697}$.

The diffusion path length z represents the characteristic length over which the evaporating liquid diffuses. It is the only parameter fitted to the measurements and its value ranges between ~0.1 and ~0.9 mm for a pan with 50-µm pinhole diameter and an open pan, respectively.

The equations are solved using the MATLAB® ODE solver for stiff differential equations, namely ode23s.

4. Results and Discussion

4.1 Effect of confinement on eicosane mass loss

Eicosane evaporation was measured over a wide range of heating rates and pinhole sizes. Figure 2 compares evaporation curves at two heating rates for open pans and two pinhole sizes and for different initial masses. These results demonstrate the importance of the various terms in Eq. 4 for different conditions.

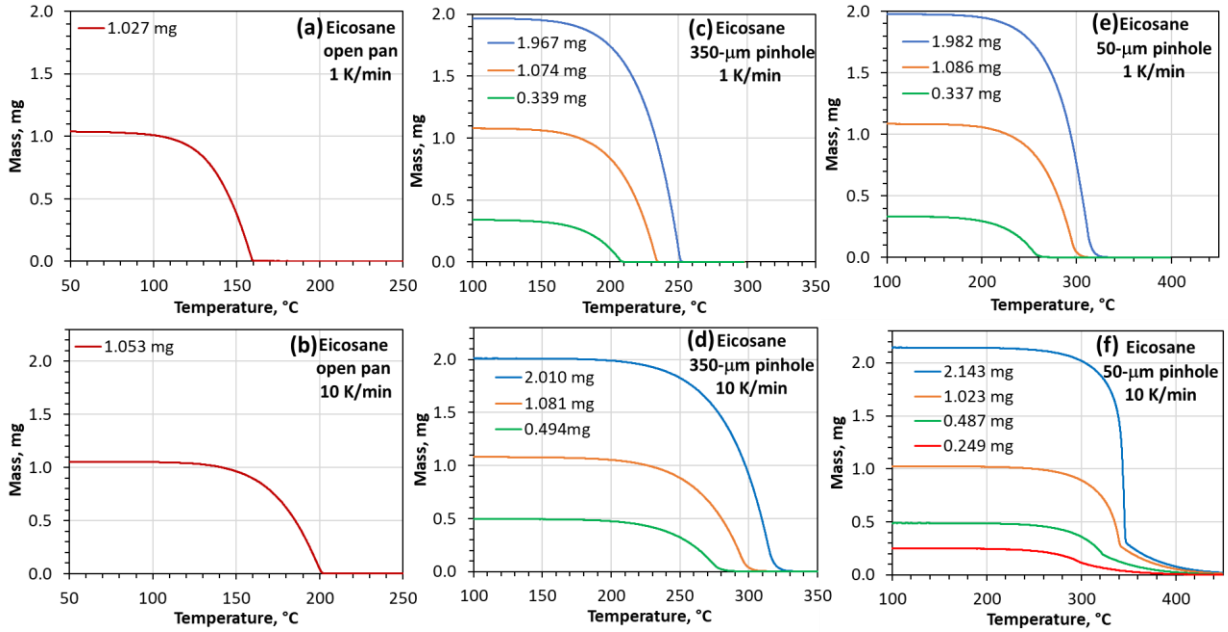

Fig 2. Eicosane mass loss measured with TGA-DSC at 1 and 10 K/min (top and bottom, respectively) in an open pan (left, panels a-b); a crucible with lid pierced with pinhole of 350 µm in diameter (middle, panels c-d); a crucible with lid pierced with pinhole of 50 µm in diameter (right, panels e-f).

In all cases, the increase in heating rate shifts the evaporation curve to higher temperature. That is simply because of the longer time available for evaporation and diffusion for a slower heating rate. The presence of a lid also shifts the evaporation to higher temperature due to additional diffusion resistance. However, the evaporation curve shape changes, also. In an open pan, the mass loss heads directly to zero. That is also the case at 1 K/min for a 350-µm pinhole, but at 10 K/min, the end of the mass loss curve curves, close to 0.1 mg, reaches zero asymptotically. The same is true for a 50-µm pinhole at both 1 and 10 K/min heating rates. This is due to a faster evaporation of eicosane than its escape by diffusion outside the pan in the surrounding atmosphere and is represented by the visible curvature at the end the exponential decay of vapor concentration inside the covered pan after the completion of evaporation. This regime is especially prominent for 2 mg in a 50-µm pinhole pan heated at 10 K/min heating rate, where there is sharp break from the completion of evaporation at the boiling point (350 °C) and transition to the diffusion regime, with a minor contribution due to vapor volume expansion. The sharp vertical drop in mass for this condition represents the transition to active boiling.

To better understand the interplay of the various processes, model predictions of liquid mass (m_L), vapor mass inside the pan (m_V), vapor mass which exited the pan (m_X) and the remaining mass ($m_{REST}= m_L + m_V$) are showed in Figure 3 in comparison to open pan and 50 µm pinhole experiments.

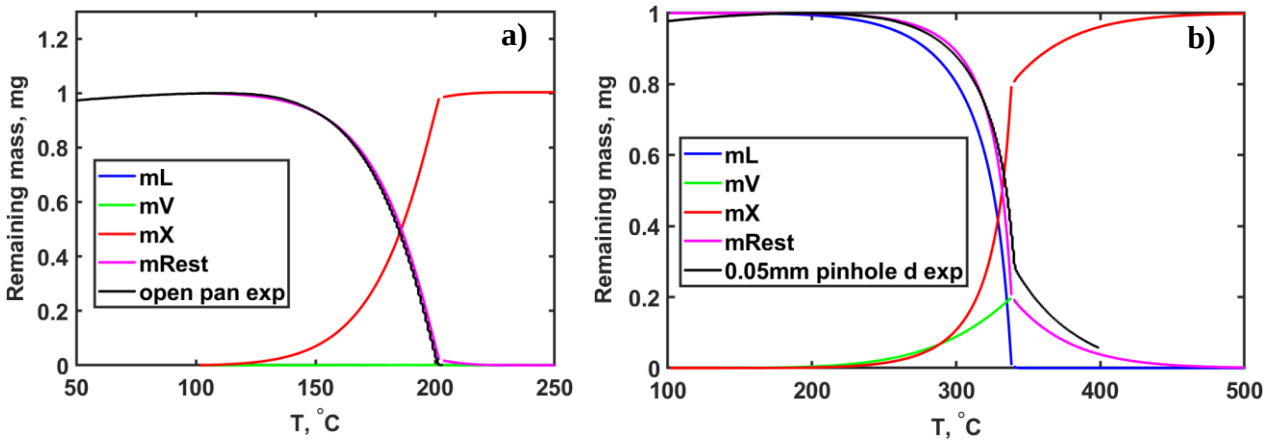

Fig. 3. Comparison between measured and predicted eicosane mass loss at 10 K/min in a) open pan; b) pan with lid pierced with pinhole of 50 µm in diameter.

The measured mass loss is equivalent to the remaining mass (m_{REST}), which for open pan experiments coincides with the liquid mass that is evaporating and immediately exiting the pan, as seen in Fig. 3a. In the case of the 50-µm pinhole, the liquid mass fully evaporates at the boiling temperature of eicosane (350 °C), while the vapor mass increases inside the pan and slowly starts to diffuse out after the completion of evaporation, changing the shape of the remaining mass profile to an exponential decay (Fig. 3b).

The only parameter fitted in order to represent the diffusion effectiveness is the diffusion path length (z), since the diffusion constant was already determined using the correlation in [26]. z is estimated to be 0.8 mm for the open pan experiment and 0.15 mm for the 50 µm pinhole experiment in Fig. 3b. z has a bigger value for open pan experiments than for experiments done with pierced lid with pinhole because the length of the diffusion pathway for the vapors differs for the two cases due to their different partial pressure in respect to the saturation pressure (see Supplemental Material).

The effect of starting mass of 0.25 mg and 2.14 mg is shown in Fig. 4 for the 50-µm pinhole experiments.

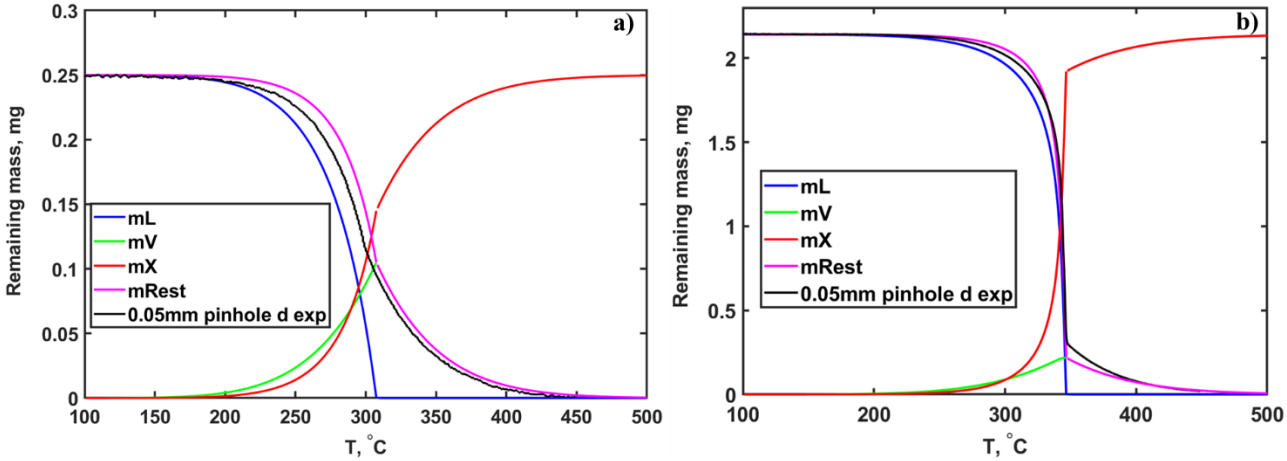

Fig. 4. Comparison between measured and predicted eicosane mass loss at 10 K/min in a crucible with lid pierced with 50 µm pinhole for a starting mass of: a) 0.25 mg and b) 2.14 mg.

Similar to the case in Fig. 3b, the liquid mass fully evaporates before all the vapors can exit the pan, slowing down the decay of remaining mass. In both cases, the diffusion path length z is around 0.15 mm, which is not different from the 1.02 mg case.

4.2 Diffusion path length dependencies

The diffusion path length z is a parameter used in the diffusion term of Eq. 4 and it is determined by fitting the mass loss of eicosane for each experiment listed in Table 1. A correlation for the diffusion path length as function as the pinhole diameter is derived and depicted in Figure 5.

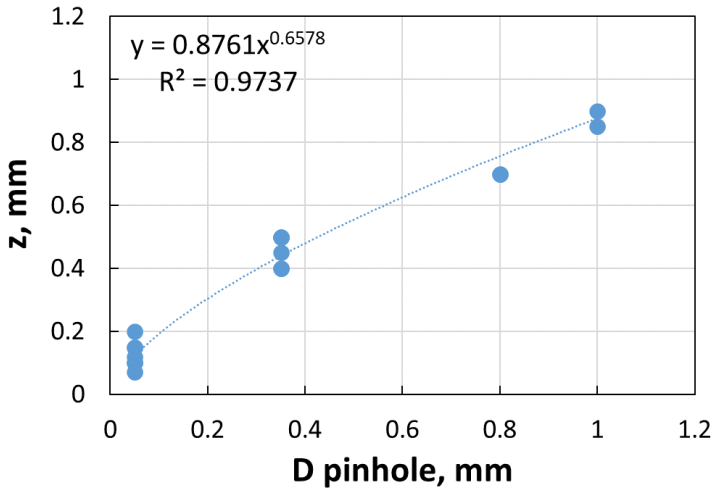

Fig. 5. Diffusion path length as function as the pinhole diameter.

It can be noted that the diffusion path length increases as the pinhole diameter increases, and the correlation derived by fitting these points is shown below:

$$z = 0.8761 * d_{pinhole}^{0.6578} \quad (5)$$

The correlation approaches the value of open pan experiments for pinhole diameters bigger than 1 mm.

Figure 6 shows the diffusion path length as function as the sample starting mass and the heating rate in panels a and b, respectively. The data are also grouped depending on the pinhole diameter used in experiments: 1 mm, 800 µm, 350 µm and 50 µm.

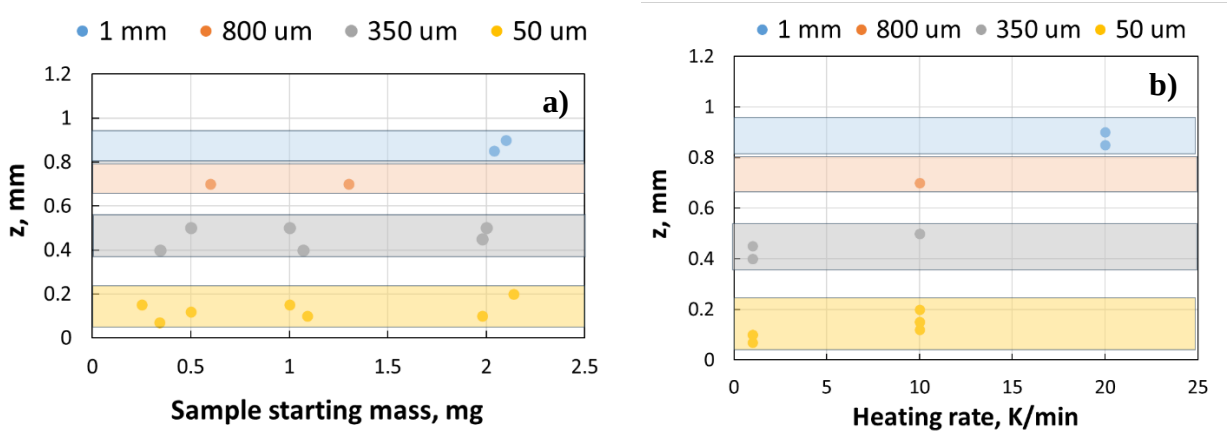

Fig. 6. Model values of diffusion path length as function as: a) starting sample mass and b) heating rate for the experiments with various pinhole diameters.

The diffusion path length values appear to be constant with sample starting mass, as well as with heating rate and they only show a dependency with pinhole diameter as already observed.

4.3 Effect of confinement on HDPE mass loss rate

The effect of diffusion on a thermal decomposition process involving chemical reaction is demonstrated in Figure 7 for HDPE. In a pinhole pan, the maximum rate of mass loss increases by about 8 °C relative to an open pan. This is roughly half the range observed in a recent compilation [27], which suggests that at least part of difference observed in the literature might be due to differences in diffusion resistance in the various works. Most of the shift occurs for a pinhole of 1.4 mm, so pinhole size is less sensitive than for eicosane itself.

The effect of a pinhole is more complex than for simple evaporation because the rate of volatilization depends on both primary and secondary pyrolysis reactions. As identified in various literature pyrolysis experiments [28-30], HDPE starts decomposing around 387 °C in a

wide range of hydrocarbons (i.e. C1 to C42) by random scission. Some of these compounds are produced above their boiling points (BP), such as n-eicosane (BP~350 °C) and are immediately vaporized and undergo diffusive release. However, products formed below their boiling point, such as n-tetracosane (BP~391 °C) or 1-hexacosene (BP~406 °C), vaporize either by slowly evaporating in the sweep gas or by breaking down to smaller products. Consequently, although it appears that the decomposition rate has slowed down as the pinhole becomes smaller, the profile shift to higher temperature is really an effect of delaying the mass release until the vapor pressure increases due to increased temperature and the decomposition to smaller products overcome the partial-pressure and diffusion resistances. Modeling this process in detail is beyond the scope of this paper, but a range of approaches for this type of problem have been described by Burnham [31, 32].

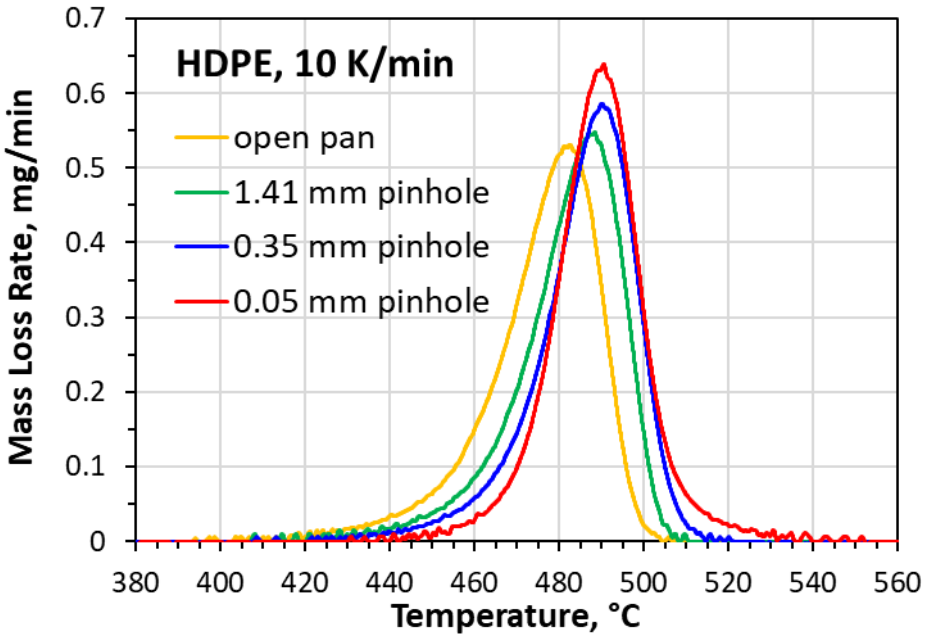

Figure 7. Rate of mass loss for pyrolysis of HDPE at 10 K/min.

5. Conclusions

The effect of confinement on the evaporation of organic materials, such as eicosane, and decomposition of organic materials, such as HDPE, is quantified in this work. Thermogravimetric experiments were performed in open crucibles and crucibles closed with a pierced lid for different heating rates and starting sample masses. A new model has been developed to account for vapor and liquid mass loss with various degrees of confinement, including various pinhole sizes. The presence of the pinhole reduced the evaporation rate of volatile starting material, and for smaller pinholes and higher heating rates the predominant role of diffusion after the end of evaporation phase was evident. The diffusion path length z

controlled the transition from kinetic-controlled evaporation to diffusion-controlled escape, and a correlation of diffusion path length with pinhole size was derived from the analysis of the experiments. The formalism we demonstrate should be widely applicable to other materials and can be extended to include the presence of reactions, which is the focus of future work.

Smaller pinhole sizes reduce the apparent decomposition rate of the organic materials in respect to open-pan experiments, as measured by their mass-loss rate, due to diffusion resistance for escape of volatile materials. For polymeric materials such as HDPE, this diffusion resistance causes a delay in the rate of mass loss from the crucible and an associated greater extent of secondary reactions that lead to lighter hydrocarbon products, which has been previously observed in other types of experiments.

Supplementary Materials

Details on the collection and interpretation of data and additional comparisons between model and experiments are included.

Acknowledgements

This work was performed under the auspices of the U.S. Department of Energy by Lawrence Livermore National Laboratory under Contract DE-AC52-07NA27344.

References

[1] N. Koga, S. Vyazovkin, A.K. Burnham, L. Favergeon, N.V. Muravyev, L.A. Pérez-Maqueda, C. Saggese, P.E. Sánchez-Jiménez, ICTAC Kinetics Committee recommendations for analysis of thermal decomposition kinetics, Thermochim. Acta, 719 (2023) 179384.

[2] C.-H. Wu, C.-Y. Chang, J.-L. Hor, S.-M. Shih, L.-W. Chen, F.-W. Chang, On the thermal treatment of plastic mixtures of MSW: pyrolysis kinetics, Waste Manage. (Oxford), 13 (1993) 221-235.

[3] A. Aboulkas, A. El Bouadili, Thermal degradation behaviors of polyethylene and polypropylene. Part I: Pyrolysis kinetics and mechanisms, Energy Convers. Manage., 51 (2010) 1363-1369.

[4] D. Shen, S. Gu, K. Luo, A.V. Bridgwater, M. Fang, Kinetic study on thermal decomposition of woods in oxidative environment, Fuel, 88 (2009) 1024-1030.

[5] M. Wolfinger, J. Rath, G. Krammer, F. Barontini, V. Cozzani, Influence of the emissivity of the sample on differential scanning calorimetry measurements, Thermochim. Acta, 372 (2001) 11-18.

[6] J. Rath, M. Wolfinger, G. Steiner, G. Krammer, F. Barontini, V. Cozzani, Heat of wood pyrolysis, Fuel, 82 (2003) 81-91.

[7] A. Anca-Couce, R. Scharler, Modelling heat of reaction in biomass pyrolysis with detailed reaction schemes, Fuel, 206 (2017) 572-579.

[8] F. Torres-Herrador, V. Leroy, B. Helber, L. Contat-Rodrigo, J. Lachaud, T. Magin, Multicomponent pyrolysis model for thermogravimetric analysis of phenolic ablators and lignocellulosic biomass, AIAA J., 58 (2020) 4081-4089.

[9] D. Lázaro, M. Lázaro, A. Alonso, D. Alvear, Effects of variation in sample mass, gas flow and lid on chemical reactions during STA measurements, in: 26th International Colloquium on the Dynamics of Explosions and Reactive Systems, 2017, pp. 1-6.
[10] G.T. Long, S. Vyazovkin, B.A. Brems, C.A. Wight, Competitive vaporization and decomposition of liquid RDX, J. Phys. Chem. B, 104 (2000) 2570-2574.
[11] R. Weese, A. Burnham, H. Turner, T. Tran, Exploring the physical, chemical and thermal characteristics of a new potentially insensitive high explosive RX-55-AE-5, J. Therm. Anal. Calorim., 89 (2007) 465-473.
[12] B. Koroglu, A.K. Burnham, I. Mashiana, A. Racoveanu, C. Arose, J.C. Crowhurst, J.G. Reynolds, Comparative analysis of sublimation and thermal decomposition of TATB, Propellants Explos. Pyrotech., (2023) e202300124.
[13] M.V. Gorn, K.A. Monogarov, I.L. Dalinger, I.N. Melnikov, V.G. Kiselev, N.V. Muravyev, Pressure DSC for energetic materials. Part 2. Switching between evaporation and thermal decomposition of 3, 5-dinitropyrazole, Thermochim. Acta, 690 (2020) 178697.
[14] I. Langmuir, The vapor pressure of metallic tungsten, Phys. Rev., 2 (1913) 329.
[15] N. Pieterse, W.W. Focke, Diffusion-controlled evaporation through a stagnant gas: estimating low vapour pressures from thermogravimetric data, Thermochim. Acta, 406 (2003) 191-198.
[16] A. Parker, R. Babas, Thermogravimetric measurement of evaporation: Data analysis based on the Stefan tube, Thermochim. Acta, 595 (2014) 67-73.
[17] R. Kendler, F. Dreisbach, R. Seif, S. Pollak, M. Petermann, Method for estimating vapour pressures based on thermogravimetric measurements with a magnetic suspension balance, Thermochim. Acta, 664 (2018) 128-135.
[18] F. Heym, B.J. Etzold, C. Kern, A. Jess, An improved method to measure the rate of vaporisation and thermal decomposition of high boiling organic and ionic liquids by thermogravimetrical analysis, Phys. Chem. Chem. Phys., 12 (2010) 12089-12100.
[19] Y. Rong, C.M. Gregson, A. Parker, Thermogravimetric measurements of liquid vapor pressure, J. Chem. Thermodyn., 51 (2012) 25-30.
[20] M. Hotta, N. Koga, Extended kinetic approach to reversible thermal decomposition of solids: A universal description considering the effect of the gaseous product and the kinetic compensation effect, Thermochim. Acta, (2024) 179699.
[21] R.D. Chirico, N. An, W.V. Steele, M.M. Strube, C. Tsonopoulos, The vapor pressure of n-alkanes revisited. New high-precision vapor pressure data on n-decane, n-eicosane, and n-octacosane, J. Chem. Eng. Data, 34 (1989) 149-156.
[22] P.J. Linstrom, W.G. Mallard, The NIST Chemistry WebBook: A chemical data resource on the internet, J. Chem. Eng. Data, 46 (2001) 1059-1063.
[23] D.C. Lewczyk, J.W. Cohan, M.L. Goetz, B.L. Trafford, R.L. Fuller, J.R. Sparks, Kinetic treatment of evaporation via thermogravimetric analysis: The case of d-limonene, Ind. Eng. Chem. Res., 59 (2020) 15069-15074.
[24] S. Vyazovkin, Kinetic effects of pressure on decomposition of solids, Int. Rev. Phys. Chem., 39 (2020) 35-66.
[25] E.N. Fuller, P.D. Schettler, J.C. Giddings, New method for prediction of binary gas-phase diffusion coefficients, Ind. Eng. Chem., 58 (1966) 18-27.
[26] K. Chae, P. Elvati, A. Violi, Effect of molecular configuration on binary diffusion coefficients of linear alkanes, J. Phys. Chem. B, 115 (2011) 500-506.

[27] R.E. Harmon, G. SriBala, L.J. Broadbelt, A.K. Burnham, Insight into polyethylene and polypropylene pyrolysis: Global and mechanistic models, Energy Fuels, 35 (2021) 6765-6775.
[28] M.J. De Witt, L.J. Broadbelt, Binary interactions between high-density polyethylene and 4-(1-naphthylmethyl) bibenzyl during low-pressure pyrolysis, Energy Fuels, 14 (2000) 448-458.
[29] A. Domınguez, C. Blanco, C. Barriocanal, R. Alvarez, M. Dıez, Gas chromatographic study of the volatile products from co-pyrolysis of coal and polyethylene wastes, J. Chromatogr. A, 918 (2001) 135-144.
[30] Z. Fu, F. Hua, S. Yang, H. Wang, Y. Cheng, Evolution of light olefins during the pyrolysis of polyethylene in a two-stage process, J. Anal. Appl. Pyrolysis, 169 (2023) 105877.
[31] A.K. Burnham, A simple kinetic model of oil generation, vaporization, coking, and cracking, Energy Fuels, 29 (2015) 7156-7167.
[32] A.K. Burnham, Correction to a simple kinetic model of oil generation, vaporization, coking, and cracking, Energy Fuels, 30 (2016) 2524-2524.